ATATÜRK ÜNİVERSİTESİ YAYINLARI
ATATURK UNIVERSITY PUBLICATIONS

Research Article *Araştırma Makalesi* DOI: 10.5281/zenodo.15739317

Investigation of The Standardization Method with Scattered X-Rays in Matrices Prepared with Different Diluters

Farklı Seyrelticilerle Hazırlanan Matrislerde Saçılan X-Işınları ile Standardizasyon Yönteminin İncelenmesi

Adem KORKMAZ
Department of Physics, Faculty of Sciences, Atatürk University, Erzurum, Türkiye

Demet YILMAZ
Department of Physics, Faculty of Sciences, Atatürk University, Erzurum, Türkiye

Abstract

In this study, it is considered to evaluate the spectral intensity ratios for different matrices to be prepared using MnO_2 and boric acid, sugar, starch, and cellulose as binders. The areas under the Compton and coherent scattering peaks with Mn Kα x-ray were calculated, and the relationship between different intensity ratios and the mean atomic number of diluted samples was investigated. 100 mCi Am-241 point radioactive source was used to excite the targets. The emitted and scattered x-rays from targets were counted by a ULEGe detector. The changes in the scattering intensity ratios of the mean atomic numbers of the matrices prepared using different diluters were plotted graphically, and the calibration curves and correlation coefficients obtained were interpreted. In addition, there is a third-degree polynomial relationship between $I_{coh}+I_{Comp}/(\mu/\rho)_{(K\alpha)}$ intensity ratio of the prepared sample group and mean atomic number. The obtained calibration curves can be used for qualitative analysis in sample groups with the same matrix.

Keywords: Qualitative analysis, Normalized scattering intensities, EDXRF, ULEGe detector.

Öz

Bu çalışmada, MnO_2 ile bağlayıcı olarak borik asit, şeker, nişasta ve selüloz kullanılarak hazırlanan farklı matrisler için spektral şiddet oranlarının değerlendirilmesi amaçlanmıştır. Mn Kα x-ışını piki ile Compton ve koherent saçılmış piklerin altındaki alanlar hesaplanarak farklı şiddet oranları ile seyreltilen numunelerin ortalama atom numarası arasındaki ilişki incelenmiştir. Hedefleri uyarmak için 100 mCi Am-241 nokta radyoaktif kaynak kullanılmıştır. Numunelerden yayınlanan ve saçılan x-ışınları ULEGe dedektörü ile sayılmıştır. Farklı seyrelticilerle hazırlanan matrislerin ortalama atom numaralarına göre saçılma şiddet oranlarındaki değişimler grafiksel olarak elde edilmiş, kalibrasyon eğrileri ve korelasyon katsayıları yorumlanmıştır. Ayrıca, hazırlanan numune grubunun $I_{coh}+I_{Comp}/(\mu/\rho)_{(K\alpha)}$ şiddet oranı ile ortalama atom numarası arasında üçüncü dereceden polinomal bir ilişki olduğu belirlenmiştir. Elde edilen kalibrasyon eğrileri, aynı matris yapısına sahip numune gruplarında kalitatif analiz amacıyla kullanılabilir.

Anahtar Kelimeler: Kalitatif analiz, Normalize edilmiş saçılma şiddetleri, EDXRF, ULEGe dedektör.

Sorumlu Yazar/Corresponding Author:
Demet Yılmaz
E-mail: *ddemir*@atauni.edu.tr

Geliş Tarihi/Received 02.02.2025
Kabul Tarihi/Accepted 08.05.2025
Yayın Tarihi/ Publication Date 27.06.2025

Cite this article
Kormaz A. & Yılmaz D. (2025) Investigation of the standardization method with scattered x-rays in matrices prepared with different dilutere. *Journal of Anatolian Physics and Astronomy,* 4(1), 1-12.

Introduction

The main principles of sample preparation technique in XRF are: reproducibility, sensitivity, simplicity, cheapness, and reliability. The proper placement of the sample is usually sufficient for qualitative X-ray spectrometric analysis. There are many parameters in the study of alloys, glasses, cements, polymers, and geological materials that have been fused, pressed, or assessed untreated. In these analyses, X-ray fluorescence spectrometry (XRF) is frequently used.

Additions to the sample, absorption, and scattering effects can be controlled by diluting the sample if they are high. When binders or diluents are used, unbound binders provide better homogeneity in irregular particle sizes and densities. It provides high packing density and a smooth surface and reduces absorption and scattering effects by dilution. Disadvantages of the binder are that light elements may have absorbing effects on analyte intensity and may give high background count due to scattering effects. Therefore, binder should be used in a minimum amount (sample should not be bound to a pure binder tray or holder). Standardization method with scattered X-rays provides compensation for tailing regions originating from multiple scattering and especially located in low energy regions of Compton scattering peaks in XRF. In addition, intensity ratios of characteristic and scattering peaks also correct the geometry factor affecting the counting efficiency of the detector. Determination of the effect of different binders used in XRF on intensity ratios of characteristic and scattering peaks will be an achievement for the literature. The purpose of determining the effect of the binders used in XRF analyses on the intensity ratios of characteristic and scattering peaks is to increase the accuracy and reliability of the measurements, to make the analysis results more precise and reliable, to improve the calibration and standardization processes of XRF devices and to ensure that the devices provide consistent results in different sample types. In addition, the compensation of tailing regions and multiple scattering in low-energy regions increases the measurement sensitivity and provides an advantage in the detection of low-concentration elements. The study contributes to the development of XRF analysis methods, enables the development of new binders and analysis techniques, and expands the applications in different industries. It provides a significant contribution to academic literature and industrial applications, and provides great benefits in XRF analyses used in fields such as material science, chemistry, and geology. More accurate and reliable analyses reduce the need for re-measurements, provide cost and time savings, and increase the efficiency of laboratories and industrial facilities. These justifications clearly show why it is important to examine the effect of the different binders used in XRF analyses on the intensity ratios of characteristic and scattering peaks and how this study will contribute to the literature.

In the literature, there are studies by absorption correction methods in XRF (Mantouvalou, 2017). Bauer developed the absorption correction approach (Bauer et al., 2024). This method makes it possible to investigate the diffusion of elements at the tooth-filling contact in three dimensions with greater accuracy. The mass absorption coefficient is used in the model. Rousseau (2006) created a mathematical adjustment for matrix effects in the analysis of X-ray fluorescence. Bowers (2019) used a simple influence factor model to rectify the matrix effect. Chebakova et al. (2021) investigated XRF properties of micro- and nanoscale particle compositions. The authors' quantitative analytical results depend on the thickness, morphology, and characteristics of the coatings. When analyzing heterogeneous materials, so-called particle size effects may be the cause of a substantial mistake. When examining samples with drastically diverse particle size distributions and light components, extreme results can even be >30% relative. In the microscale region, X-ray fluorescence intensity rose as particle size shrank (Finkel'shtein & Gunicheva, 2008). Sitko (2009) investigated matrix effects in samples of less than infinite thickness. Yılmaz and Boydaş (2018) studied the scattering peaks for matrix effect correction in WDXRF analysis. For quantitative X-ray spectrometry, Uzunoğlu et al. (2015) suggested employing the characteristic and scattering peaks. Tee et al. (2024) studied the method to fit Compton profiles in X-ray fluorescence (XRF) spectroscopy. In assessing the areas under the Compton peaks acquired at various energies, researchers in this work underlined the significance of identifying the background region and its energy dependence. The background form of an XRF spectrum and the line shape of the fluorescence peaks may also be influenced by the scattered X-rays, as a very small fraction of fluorescent X-rays scatter in the sample or instrument before they reach the detector. A model for Compton peaks in energy-dispersive X-ray fluorescence spectra was created by Van Gysel et al. (2003). The model uses Monte Carlo simulations to systematically investigate peak morphology. Perez et al. (2024) looked into wine adulteration using the effective atomic number and the Compton/Rayleigh intensity ratio. Büyükyıldız (2016) determined effective atomic numbers (Z_{eff}) of Fe_xCu_{1-x} binary ferro alloys by using the Rayleigh to Compton scattering ratio. Hodoroaba and Rackwitz (2014) used the Compton to Rayleigh intensity ratio, which has a high specificity to the mean atomic number, to obtain additional information about the chemical composition of the sample using XRF).

In this work, we used the scattered peak ratio method. It is planned to evaluate the spectral intensity ratios for different matrices to be prepared using the oxidized compound (MnO_2) of an element with medium atomic number and boric acid, sugar, starch and cellulose as binders. The calibration curves drawn from the intensity ratios $I_{sc_{(K\alpha)}} = I_{coh}/2(\mu/\rho)_{K_{\alpha_1}} + I_{Comp}/2(\mu/\rho)_{K_{\alpha_1}} + (\mu/\rho)_{59,54}$ and $(\mathrm{I_{coh}} + \mathrm{I_{Comp}})/(\mu/\rho)_{K_\alpha}$ versus mean atomic number in EDXRF system. Targets of various concentrations were excited by 59.54 keV γ-rays from a 100 mCi Am-241 point radioactive source. The emitted and scattered X-rays by samples were counted by an ULEGe detector.

Experimental

In this study, a conical lead collimator was used to provide the source and detector to see the sample in the 45° geometry in Figure 1. The experimental system used includes a ULEGe (Ultra Low Energy Germanium Detector), and the photograph of the experimental system is shown in Figure 2. The physical and electrical characteristics of the ULEGe detector is given in Table 1. The hydraulic press used in the production of the samples is given. The samples were pressed using a 13 mm die set using 7 tons of pressure. A spectrum taken from a MnO_2 sample diluted with H_3BO_3 in the EDXRF system is given in Figure 3. The radioactive source used is a 100 mCi Am-241 source.

Table 1. Physical and electrical characteristic of the ULEGe detector

Window	Beryllium; 25 µm
Energy resolution (FWHM)	140 eV at 5.9 keV, 520 eV at 122 keV
Active diameter	8 mm
Active area	50 mm^2
Thickness	5 mm
Distance from window	5 mm
Bias voltage	-500 Vdc
Depletion voltage	-300 Vdc

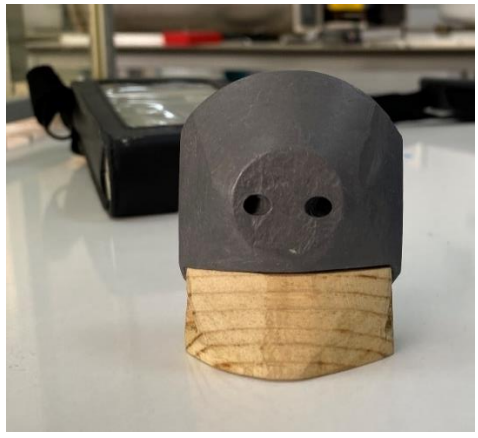

Figure 1. Lead collimator.

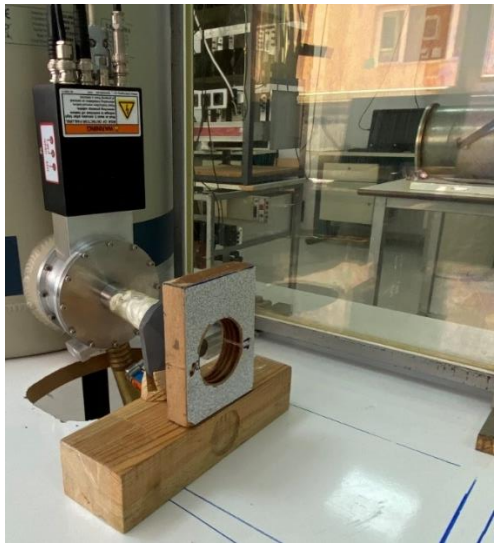

Figure 2. Experimental system.

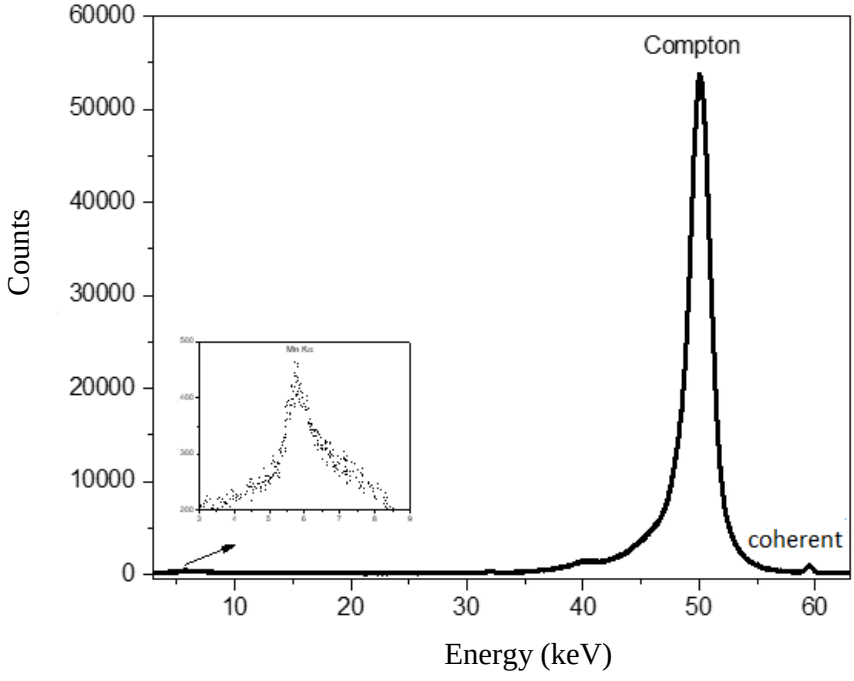

Figure 3. The XRF spectrum of MnO_2 diluted by H_3BO_3.

Preparation of samples

In this study, the chemical compound MnO_2 was diluted with sugar, starch, cellulose and boric acid using the dilution technique. Samples with different mean atomic numbers were obtained with each diluent. The mean atomic number of the diluents used is found with the expression

$$\bar{Z}_c = \frac{\sum_i n_i Z_i}{n} \quad (1)$$

where *n* is the total number of atoms in the diluent, n_i is the atomic number of the *i*th element in the diluent, and Z_i is the atomic number of the ith element in the diluent. The percentage concentrations of the diluent forming the sample and the chemical compound used (MnO_2) were calculated with the expression:

$$C_{b(c)}\% = \frac{m_{b(c)}}{m_b + m_c} \times 100 \tag{2}$$

where m_b is the mass of the compound and m_c is the mass of the diluent. The mean atomic number of the samples can be calculated from the expression:

$$\bar{Z}_s = \bar{Z}_b \times C_b + \bar{Z}_c \times C_c \tag{3}$$

Here, $\bar{Z}_s$ is the mean atomic number of the sample, $\bar{Z}_b$ and $\bar{Z}_c$ are the mean atomic number of the compound and diluent used, C_b and C_c are the percentage concentrations of the compound and diluent. The mass amounts, percentage concentrations, sample thicknesses, and mean atomic numbers of the samples prepared with the MnO_2 compound diluted with fourteen different diluents to be used in the study are given in Tables 2 -5. The total scattered intensity at a specific wavelength is expressed as follows (E.P. Bertin, 1975):

$$I_{sc} = \frac{I_{coh}}{2(\mu/\rho)_\lambda} + \frac{I_{Comp}}{2(\mu/\rho)_\lambda + (\mu/\rho)_{\lambda-\Delta\lambda}} \tag{4}$$

I_{coh} ve I_{Comp} in the expression indicate the areas under the coherent and Compton peaks. $(\mu/\rho)_\lambda$ is the mass absorption coefficient of the sample at a specific wavelength (e.g. K_α) and $(\mu/\rho)_{\lambda-\Delta\lambda}$) is the mass absorption coefficient of the sample at the excitation photon energy. In this work, the total scattering intensity was calculated.

$$I_{sc_{(K_\alpha)}} = \frac{I_{coh}}{2(\mu/\rho)_{K\alpha_1}} + \frac{I_{Comp}}{2(\mu/\rho)_{K\alpha_1} + (\mu/\rho)_{59,54}} \tag{5}$$

In addition, the intensity ratios $(I_{coh} + I_{Comp})/(\mu/\rho)_{K_\alpha}$ were also calculated. The mass absorption coefficients of the samples prepared at a specific X-ray energy were calculated from the EpiXS program (Hila et al., 2021). The changes in the mean atomic number and scattering intensity of the samples obtained with the MnO_2 compound diluted with different diluents are given in Figure 4-11.

Table 2. The properties of prepared samples (MnO_2/H_3BO_3)

Sample No	m_b (g)	m_c (g)	C_b (%)	C_c (%)	Mass Thickness (g/cm²)	$(\mu/\rho)_{6\ keV}$ (cm²/g)	$(\mu/\rho)_{59.54\ keV}$ (cm²/g)	$\bar{Z}_s$
1	0.60	0.00	1.00	0.00	0.93	5.62	0.755	13.66
2	0.57	0.03	0.95	0.05	0.99	5.45	0.727	12.32
3	0.54	0.06	0.90	0.10	1.00	5.29	0.699	11.23
4	0.51	0.09	0.85	0.15	0.97	5.11	0.671	10.33
5	0.48	0.12	0.80	0.20	1.00	4.95	0.643	9.030
6	0.00	0.60	0.75	0.25	2.60	4.78	0.615	4.090

Table 3. The properties of prepared samples (MnO_2/starch)

Sample No	m_b (g)	m_c (g)	C_b (%)	C_c (%)	Mass Thickness (g/cm²)	$(\mu/\rho)_{6\ keV}$ (cm²/g)	$(\mu/\rho)_{59.54\ keV}$ (cm²/g)	$\overline{Z}_s$
1	0.60	0.00	1.00	0.00	0.93	5.62	0.755	13.66
2	0.57	0.03	0.95	0.05	0.96	5.44	0.727	11.31
3	0.54	0.06	0.90	0.10	0.96	5.25	0.699	10.85
4	0.51	0.09	0.85	0.15	0.94	5.09	0.671	9.880
5	0.48	0.12	0.80	0.20	0.55	4.88	0.643	9.220
6	0.00	0.60	0.75	0.25	2.40	4.69	0.615	4.090

Table 4. The properties of prepared samples (MnO_2/sugar)

Sample No	m_b (g)	m_c (g)	C_b (%)	C_c (%)	Mass thickness (g/cm²)	$(\mu/\rho)_{6\ keV}$ (cm²/g)	$(\mu/\rho)_{59.54\ keV}$ (cm²/g)	$\overline{Z}_s$
1	0.60	0.00	1.00	0.00	0.93	5.62	0.755	13.66
2	0.57	0.03	0.95	0.05	1.00	5.44	0.727	11.31
3	0.54	0.06	0.90	0.10	1.00	5.25	0.699	10.85
4	0.51	0.09	0.85	0.15	0.88	5.09	0.671	9.880
5	0.48	0.12	0.80	0.20	0.96	4.88	0.643	9.220
6	0.00	0.60	0.75	0.25	2.00	4.69	0.615	4.090

Table 5. The properties of prepared samples (MnO_2/cellulose)

Sample No	m_b (g)	m_c (g)	C_b (%)	C_c (%)	Mass thickness (g/cm²)	$(\mu/\rho)_{6\ keV}$ (cm²/g)	$(\mu/\rho)_{59.54\ keV}$ (cm²/g)	$\overline{Z}_s$
1	0.60	0.00	1.00	0.00	0.93	5.62	0.755	13.66
2	0.57	0.03	0.95	0.05	0.77	5.43	0.727	11.31
3	0.54	0.06	0.90	0.10	1.00	5.25	0.699	10.85
4	0.51	0.09	0.85	0.15	0.78	5.06	0.671	9.880
5	0.48	0.12	0.80	0.20	0.69	4.87	0.643	9.220
6	0.00	0.60	0.75	0.25	3.00	4.68	0.615	4.090

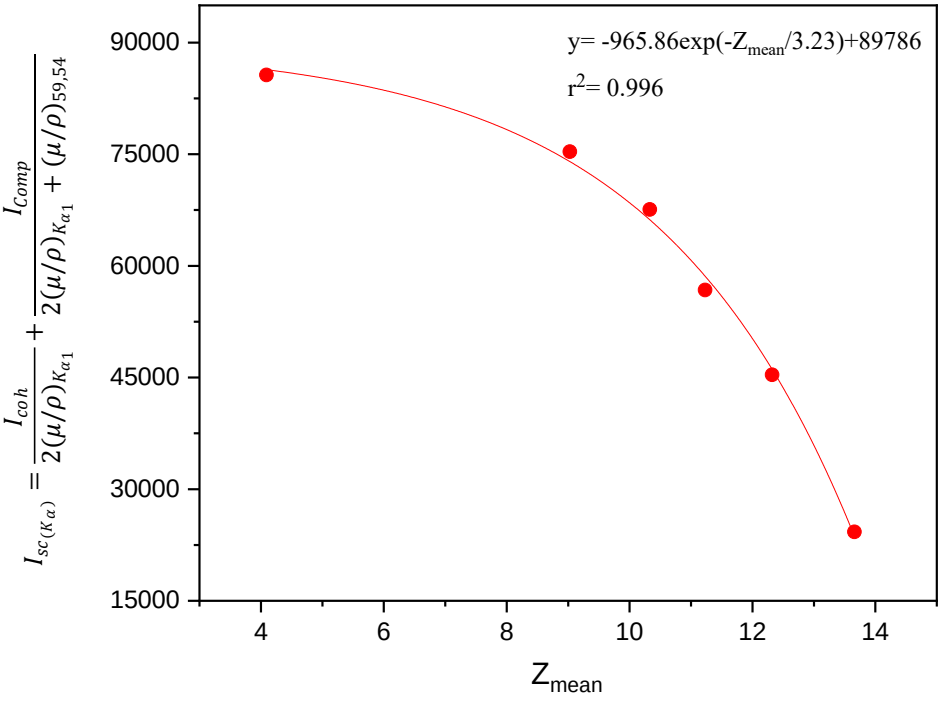

Figure 4. Variation of the total scattering intensity ratio with the mean atomic number for the MnO_2/H_3BO_3 sample group.

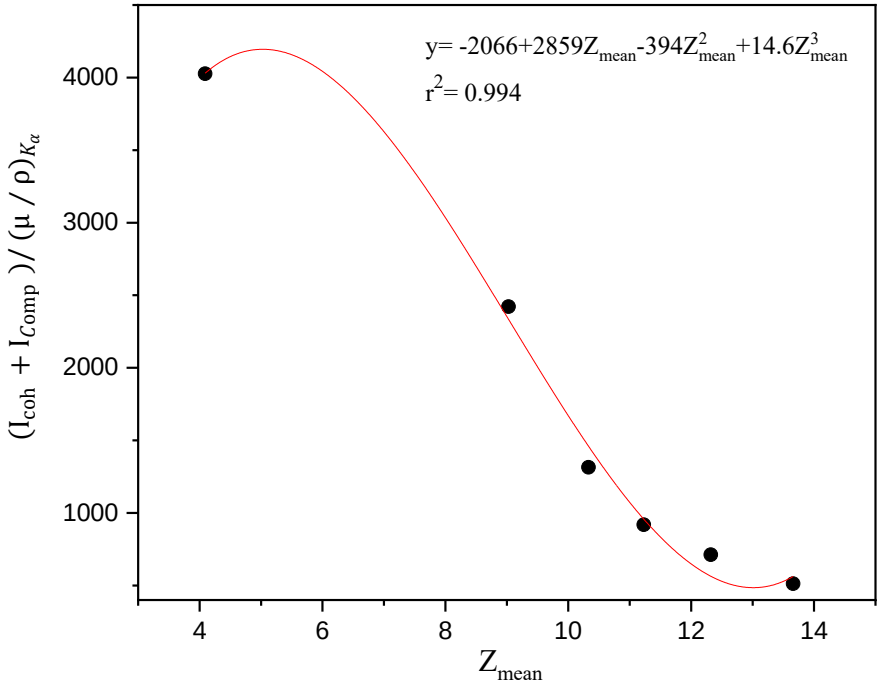

Figure 5. Variation of the intensity ratio $(I_{coh}+I_{Comp})/(\mu/\rho)_{(K\alpha)}$ with the mean atomic number for the MnO_2/H_3BO_3 sample group.

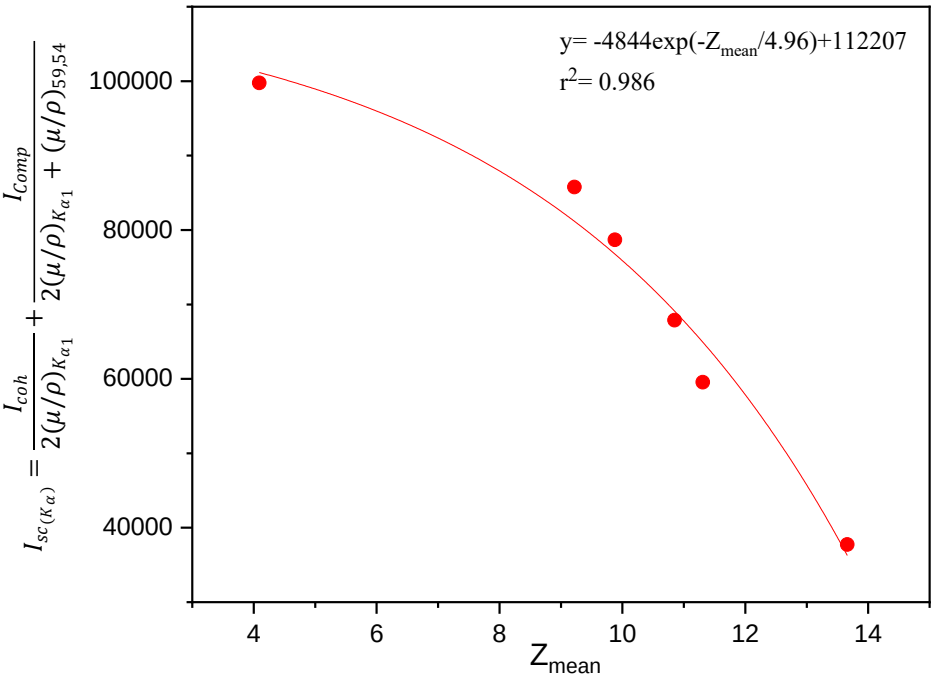

Figure 6. Variation of the total scattering intensity ratio with the mean atomic number for the MnO_2/starch sample group.

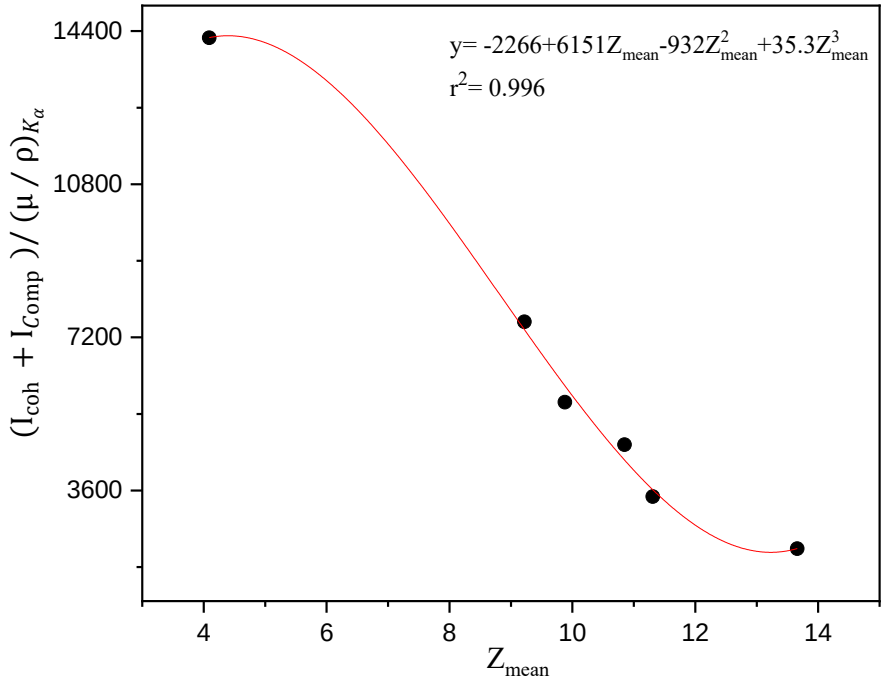

Figure 7. Variation of the intensity ratio $(I_{coh}+I_{Comp})/(\mu/\rho)_{(K\alpha)}$ with the mean atomic number for the MnO_2/starch sample group.

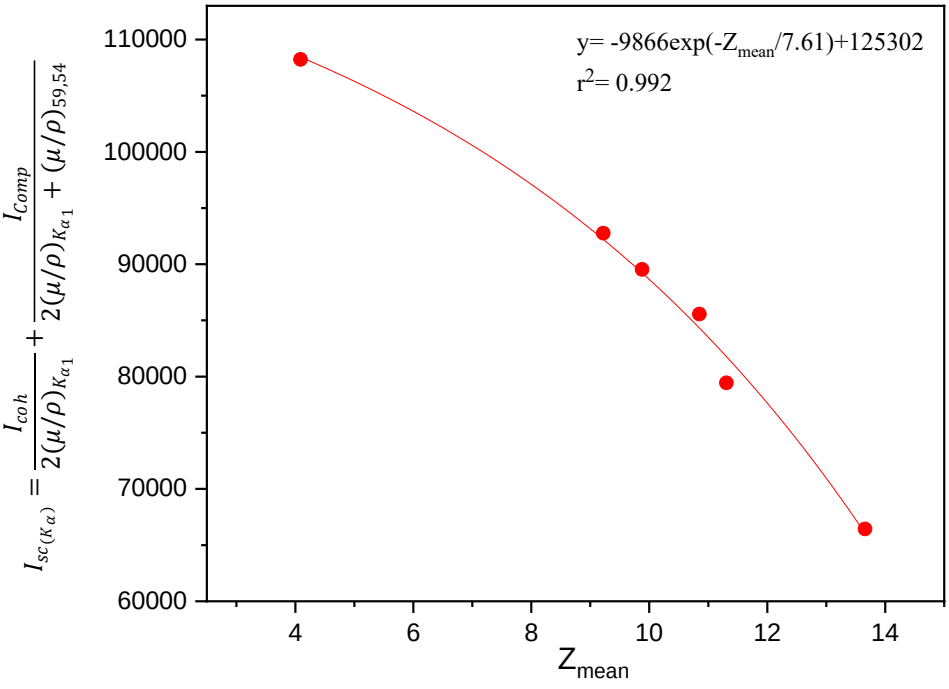

Figure 8. Variation of the total scattering intensity ratio with the mean atomic number for the MnO_2/sugar sample group.

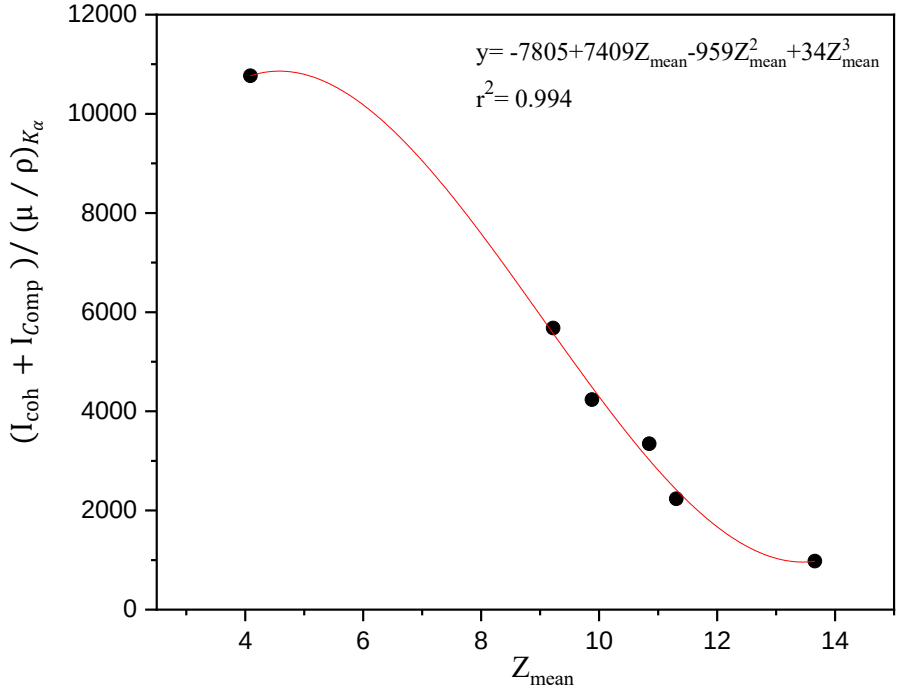

Figure 9. Variation of the intensity ratio $(I_{coh}+I_{Comp})/(\mu/\rho)_{(K\alpha)}$ with the mean atomic number for the MnO_2/sugar sample group.

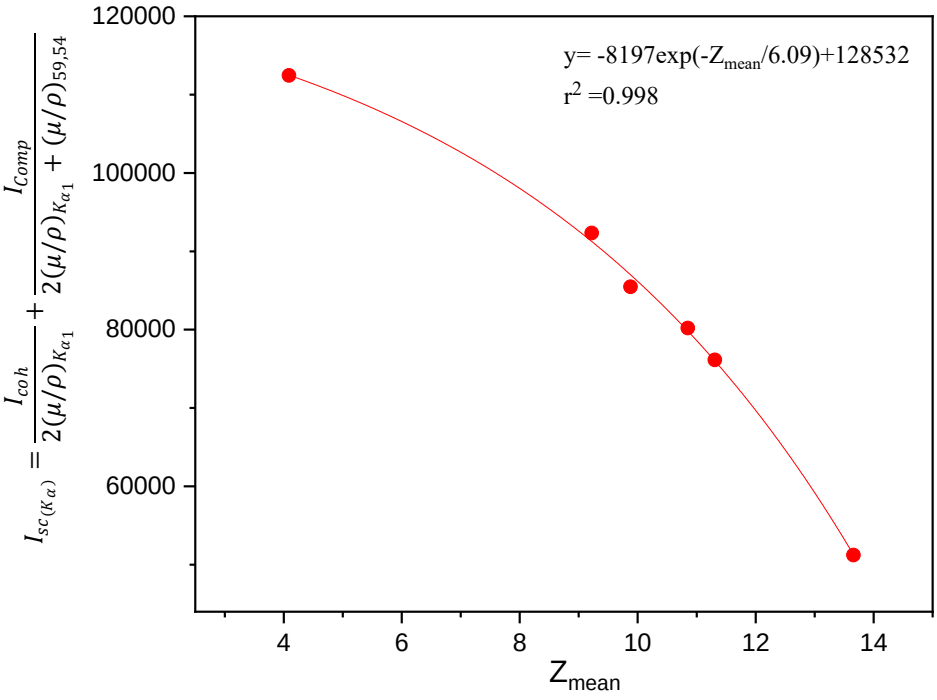

Figure 10. Variation of the total scattering intensity ratio with the mean atomic number for the MnO_2/cellulose sample group.

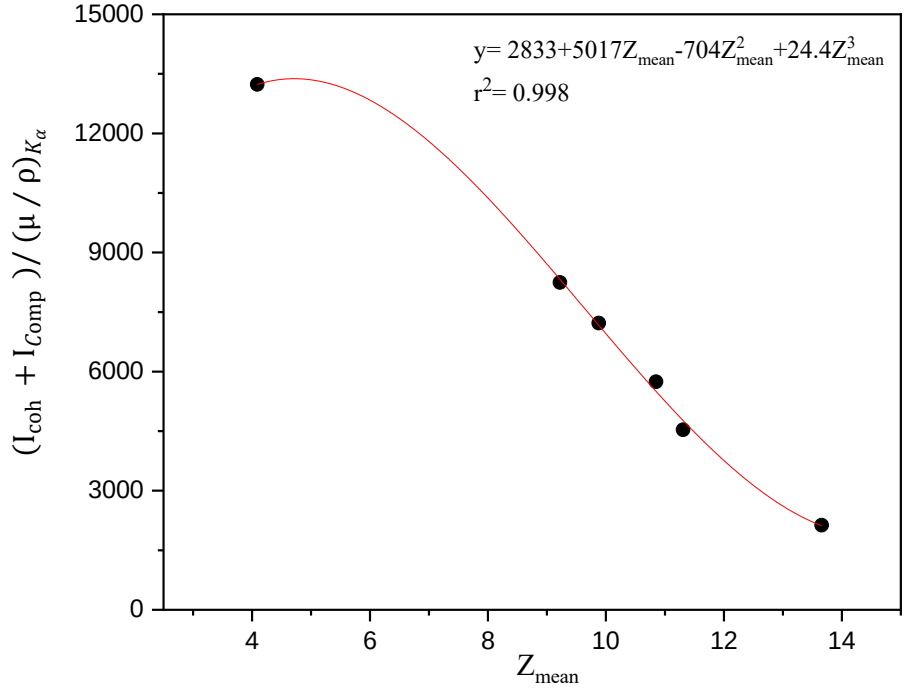

Figure 11. Variation of the intensity ratio $(I_{coh}+I_{Comp})/(\mu/\rho)_{(K\alpha)}$ with the mean atomic number for the MnO_2/cellulose sample group.

Results and Discussion

The main principles of sample preparation technique in XRF are reproducibility, sensitivity, simplicity, cheapness, and rapidity. For qualitative X-ray spectrometric analysis, it is usually sufficient to place the sample in the appropriate place. However, for quantitative analysis, many conditions and methods are important in preparation and form. For example, sample errors (homogeneity, surface texture, particle size, and inhomogeneity in distribution, amount of porosity, surface representativeness of the sample, etc.) should be reduced. Additions should be made to the sample. If absorption-intensification effects are high, internal standards should be added, matrix masking agents should be added, or the sample should be diluted, internal control standards or intensity-reference standards should be added, or standard-addition or standard-dilution methods should be used. The sample dilution method was used in this study. Binders that can be used in XRF to reduce absorption and amplification effects or to compensate for deviations from linearity that may arise from these effects are given in the literature as cellulose, Li_2CO_3, boric acid (H_3BO_3), carbon, stearic acid ($C_{17}H_{35}COOH$), polyvinyl alcohol (PVA), commercial soap and detergent powders, Al, starch, sugar and filter or chromatographic paper. Binders should be used as little as possible, and their addition to the sample should not exceed 5-20%. Based on this literature information, in this study, cellulose, boric acid (H_3BO_3), starch, and granulated sugar were used as binders in order to create different matrices with MnO_2 compound. The effect of binders on scattering and characteristic peaks was investigated using different peak ratio methods (standardization with scattered X-rays) against the mean atomic number. When Figure 4, 6, 8 and 10, where the changes in the total scattering intensity ratio in Mn Kα energy with the mean atomic number are given for the MnO_2/H_3BO_3, MnO_2/starch, MnO_2/sugar and MnO_2/cellulose sample groups, are examined, it is seen that there is an exponential relationship between the total scattering intensity ratios and the mean atomic number of the formed samples and this relationship is compatible with the correlation coefficient given in the graphs. However, when Figure 5, 7, 9 and 11, where the changes in the $(I_{coh} + I_{Comp})/(\mu/\rho)_{K_\alpha}$ intensity ratio with the mean atomic number are given for the MnO_2/H_3BO_3, MnO_2/starch, MnO_2/sugar and MnO_2/cellulose sample groups, are examined, it is seen that there is a third-degree polynomial relationship between the total scattering intensity ratios and the mean atomic number of the formed samples and this relationship is compatible with the correlation coefficients given in the graphs. The correlation coefficients obtained show that the relevant calibration curves can be used in qualitative analyses.

While preparing the sample, the smaller particles with the same density are located at the bottom. The binders used in this study were sieved to minimize the errors that will come from the particle size effect. Since a light matrix sample was created, it was not possible to look at the L_α/K_α or M_α/K_α intensity ratios of the samples given in the literature. However, it is an achievement for the literature to determine that the particle size effect is minimized in light matrix samples by looking at the characteristic and scattering peak intensity ratios ($I_{K\alpha}/I_{Comp}$).

Conclusion

All binders used in this study are organic structures composed of light elements. Compton scattering is always dominant in light elements. The additional concentration of the binder added to the samples should not exceed 20%, which is known in the literature. In the study, Mn Kα and Compton scattering peak intensity ratios were controlled at each dilution stage. Since the increase in binder concentration will increase the amplification effect in the sample, this will bring an unwanted error to the spectra in XRF analyses. Although binders other than H_3BO_3 have the same chemical structure ($C_6H_{10}O_5$), their crystal structures are different, so their packing fractions are different from each other. Although the briquetting pressure was kept the same in all samples in this study, the changing intensity ratios show that the analyte-line intensity measured in the diluted samples changes with the sample packing fraction of the measured wavelength path length. The existence of this effect in compounds with the same chemical structure was revealed in the same matrix samples prepared by the dilution method. In XRF, there is a concentration range where the binder types used are effective in analyte line intensity, such that the analyte-line intensity increases with decreasing particle size at a given briquetting pressure, and the intensity increases with increasing briquetting pressure at the same particle size. This makes a significant contribution to the analyte intensification effect of the sample. However, since the software programs that give absorption coefficients do not contain physical information about chemical bonds, although they give the same absorption coefficient value to similar chemical structures, the fact that different contributions are obtained in intensity ratios in the examination of XRF spectra also points to the deficiency in the existing programs.

Hakem Değerlendirmesi: *Dış bağımsız.*
Yazar Katkıları: *Fikir-DY; Tasarım-DY; Denetleme DY-; Kaynaklar-AK; Veri Toplanması ve/veya İşlemesi AK; Analiz ve/ veya Yorum DY; Literatür Taraması AK; Yazıyı Yazan-DY; Eleştirel İnceleme-DY.*
Çıkar Çatışması: *Yazarlar, çıkar çatışması olmadığını beyan etmiştir.*
Finansal Destek: *Bu çalışma için herhangi bir kurumdan finansal destek alınmamıştır.*
Peer-review: *Externally peer-reviewed.*
Author Contributions: Concept - DY; Design - DY; Supervision - DY; Resources - DY; Materials - AK; Data Collection and/or Processing - AK; Analysis and/or Interpretation - DY; Literature Search - AK; Writing Manuscript - DY; Critical Review - DY;
Conflict of Interest: *The authors have no conflicts of interest to declare.*
Financial Disclosure: *No financial support was received from any institution for this study.*

References

Bauer, L.J., Wieder, F., Truong, V., Förste, F., Wagener, Y., Jonas, A., Praetz, S., Schlesiger, C., Kupsch, A., Müller, B.R., Kanngießer, B., Zaslansky, P. & Mantouvalou, I. (2024). Absorption Correction for 3D Elemental Distributions of Dental Composite Materials Using Laboratory Confocal Micro-X-ray Fluorescence Spectroscopy. *Analytical Chemistry*, 96, 8441–8449. https://doi.org/10.1021/acs.analchem.4c00116.

Bowers, C. (2019). Matrix Effect Corrections in X-ray Fluorescence Spectrometry. *Journal of Chemical Education,* 96, 2597–2599. https://doi.org/10.1021/acs.jchemed.9b00630.

Büyükyıldız, M. (2016). Determination of the effective atomic numbers of Fe_xCu_{1-x} binary ferroalloys using a nondestructive technique: Rayleigh-to-Compton scattering ratio. *Turk J. Phys.,* 40, 278-286. 10.3906/fiz-1603-25.

Bertin, E.P. (1975). Principles and Practice of X-Ray Spectrometric Analysis. Plenum Press.

Chebakova, K.A., Dzidziguri, E.L., Sidorova, E.N., Vasiliev, A.A., Ozherelkov, D.Y., Pelevin, I.A., Gromov, A.A. & Nalivaiko, A.Y. (2021). X-ray Fluorescence Spectroscopy Features of Micro- and Nanoscale Copper and Nickel Particle Compositions. *Nanomaterials,* 11, 2388. https://doi.org/10.3390/nano11092388.

Finkel'shtein, A.L. & Gunicheva, T.N. (2008). Description of the dependence of intensity of x-ray fluorescence on the particle size of powder samples and pulp during x-ray fluorescent analysis. *Inorganic Materials,* 44, 1567–1571. https://doi.org/10.1134/S0020168508140136.

Hila, F.C., Asuncion-Astronomo, A., Dingle, C.A.M., Jecong, J.F.M., Javier-Hila, A.M. V., Gili, M.B.Z., Balderas, C. V., Lopez, G.E.P., Guillermo, N.R.D. & Amorsolo, A. V. (2021). EpiXS: A Windows-based program for photon attenuation, dosimetry and shielding based on EPICS2017 (ENDF/B-VIII) and EPDL97 (ENDF/B-VI.8). *Radiation Physics and Chemistry,* 182, 109331. https://doi.org/10.1016/j.radphyschem.2020.109331.

Hodoroaba, V.D. & Rackwitz, V. (2014). Gaining improved chemical composition by exploitation of Compton-to-Rayleigh intensity ratio in XRF analysis. *Anal. Chem.,* 86, 6858-6864. https://doi.org/10.1021/ac5000619.

Mantouvalou, I., Lachmann, T., Singh, S.P., Vogel-Mikuš, K. & Kanngießer, B. (2017). Advanced Absorption Correction for 3D Elemental Images Applied to the Analysis of Pearl Millet Seeds Obtained with a Laboratory Confocal Micro X-ray Fluorescence Spectrometer. *Analytical Chemistry,* 89, 5453–5460. https://doi.org/10.1021/acs.analchem.7b00373.

Pérez, S., Vasquez, R., Pascual, G., Araya, J., Neira, J. & Cespedes-Acuña, C.L. (2024). Toward the authentication of wines of Itata valley denomination of origin through total reflection x-ray fluorescence (TXRF) method for testing adulteration. A novel valuable tool by using Compton/Rayleigh scattering signals in wines. *Food Bioscience,* 61, 104475. https://doi.org/10.1016/j.fbio.2024.104475.

Rousseau, R.M. (2006). Corrections for matrix effects in X-ray fluorescence analysis—A tutorial. *Spectrochimica Acta Part B: Atomic Spectroscopy,* 61, 759–777. https://doi.org/10.1016/j.sab.2006.06.014.

Sitko, R. (2009). Quantitative X-ray fluorescence analysis of samples of less than 'infinite thickness': Difficulties and possibilities. *Spectrochimica Acta Part B: Atomic Spectroscopy,* 64, 1161–1172. https://doi.org/10.1016/j.sab.2009.09.005.

Tee, B.P.E., Ganly, B., Mcllquham, J.D., Giang, P. & Van Haarlem, Y. (2024). Fitting Compton peaks from first principles in x-ray fluorescence spectra. *X-Ray Spectrometry*, https://doi.org/10.1002/xrs.3441.

Uzunoğlu, Z., Yilmaz, D. & Şahin, Y. (2015). Quantitative x-ray spectrometric analysis with peak to Compton ratios. *Radiation Physics and Chemistry,* 112. https://doi.org/10.1016/j.radphyschem.2015.03.039.

Van Gysel, M., Lemberge, P. & Van Espen, P. (2003). Description of Compton peaks in energy-dispersive x-ray fluorescence spectra. *X-Ray Spectrometry,* 32, 139–147. https://doi.org/10.1002/xrs.628.

Yılmaz, D. & Boydaş, E. (2018). The use of scattering peaks for matrix effect correction in WDXRF analysis. *Radiation Physics and Chemistry,* 153, 17–20. https://doi.org/10.1016/j.radphyschem.2018.08.035.